Cell

Resource

A Quantitative Chaperone Interaction Network Reveals the Architecture of Cellular Protein Homeostasis Pathways

Mikko Taipale,[1] George Tucker,[2,3] Jian Peng,[2,3] Irina Krykbaeva,[1] Zhen-Yuan Lin,[4] Brett Larsen,[4] Hyungwon Choi,[5] Bonnie Berger,[2,3] Anne-Claude Gingras,[4,6,*] and Susan Lindquist[1,7,8,*]

[1]Whitehead Institute for Biomedical Research, Cambridge, MA 02114, USA
[2]Computer Science and Artificial Intelligence Laboratory, Massachusetts Institute of Technology, Cambridge, MA 02139, USA
[3]Department of Mathematics, Massachusetts Institute of Technology, Cambridge, MA 02139, USA
[4]Centre for Systems Biology, Lunenfeld-Tanenbaum Research Institute at Mount Sinai Hospital, Department of Molecular Genetics, University of Toronto, Toronto, ON M5G 1X5, Canada
[5]National University of Singapore and National University Health System, Singapore 117597, Singapore
[6]Department of Molecular Genetics, University of Toronto, Toronto, ON M5S 1A8, Canada
[7]Department of Biology, Massachusetts Institute of Technology, Cambridge, MA 02139, USA
[8]Howard Hughes Medical Institute, Cambridge, MA 02139, USA
*Correspondence: gingras@lunenfeld.ca (A.-C.G.), lindquist_admin@wi.mit.edu (S.L.)
http://dx.doi.org/10.1016/j.cell.2014.05.039

SUMMARY

Chaperones are abundant cellular proteins that promote the folding and function of their substrate proteins (clients). In vivo, chaperones also associate with a large and diverse set of cofactors (cochaperones) that regulate their specificity and function. However, how these cochaperones regulate protein folding and whether they have chaperone-independent biological functions is largely unknown. We combined mass spectrometry and quantitative high-throughput LUMIER assays to systematically characterize the chaperone-cochaperone-client interaction network in human cells. We uncover hundreds of chaperone clients, delineate their participation in specific cochaperone complexes, and establish a surprisingly distinct network of protein-protein interactions for cochaperones. As a salient example of the power of such analysis, we establish that NUDC family cochaperones specifically associate with structurally related but evolutionarily distinct β-propeller folds. We provide a framework for deciphering the proteostasis network and its regulation in development and disease and expand the use of chaperones as sensors for drug-target engagement.

INTRODUCTION

Perturbation of the proteostasis network has been implicated in many diseases ranging from neurodegeneration to cancer and Mendelian disorders (Powers et al., 2009). At the same time, preclinical models and clinical results obtained with drugs that target central modules of the network, such as proteasome and Hsp90 inhibitors, have shown that targeting this network has high therapeutic potential (Trepel et al., 2010). It is clear, however, that we need a more detailed understanding of the proteostasis network to decipher exactly how it is perturbed in disease and to develop more effective and specific therapeutics.

Chaperones are the most prominent class of proteins that shape this network. They transiently bind thousands of substrate proteins (clients) and promote their folding, trafficking, and degradation (Saibil, 2013). Systematic proteomic approaches have started to uncover the client protein ensembles of chaperones (Calloni et al., 2012; Yam et al., 2008; Zhao et al., 2005). However, previous studies employed widely varying methods and model organisms, which makes it challenging to quantitatively compare results and integrate them into a coherent model. Perhaps more importantly, however, chaperones do not function in isolation. Rather, they dynamically associate with a diverse set of cofactors, or cochaperones. Cochaperones provide a host of auxiliary functions to chaperones, ranging from regulating the rate of client release to recruiting specific clients to the core chaperone (Echtenkamp and Freeman, 2012). A growing body of evidence suggests that cochaperones play much more than a supportive role. Some "cochaperones" possess intrinsic chaperone activity themselves (Freeman et al., 1996) and others independently regulate cellular processes that are distinct from those of the canonical chaperones (Echtenkamp et al., 2011). Yet, both the client-protein specificity and possible chaperone-independent functions of most cochaperones remain enigmatic.

Here, we use a systematic and integrative approach to survey the physical interaction landscape of all known Hsp90 cochaperones and several known Hsp70 cochaperones. We combine mass spectrometry (MS) and quantitative LUMIER assays to characterize the client specificity of cochaperones and begin to decipher the proteostasis network as a whole.

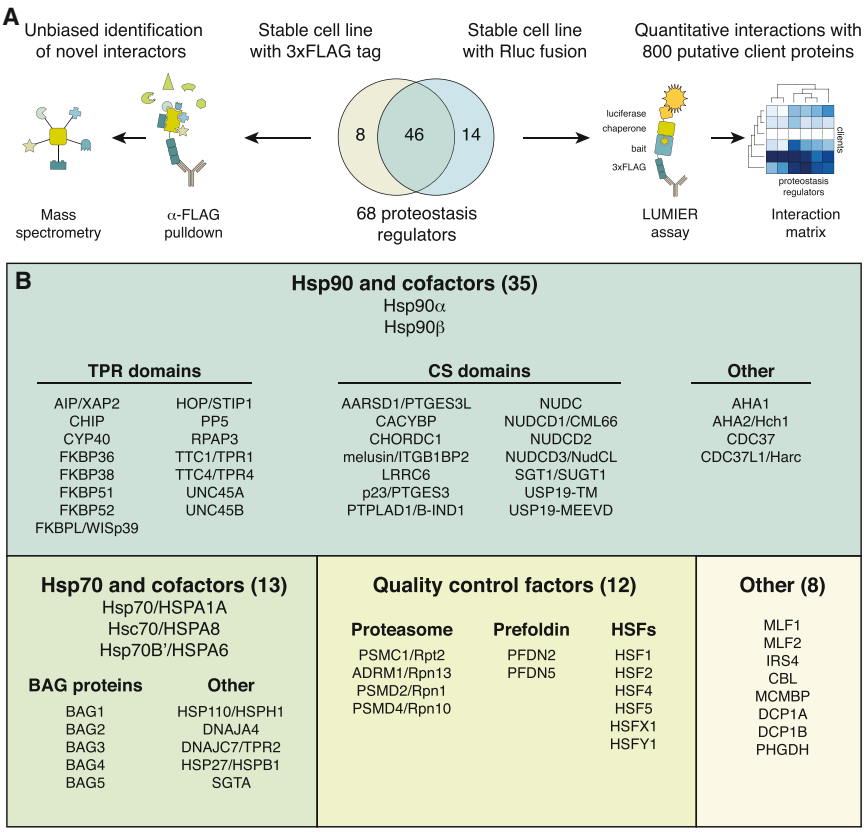

Figure 1. Two-Pronged Approach for Characterizing the Proteostasis Network in Human Cells

(A) Sixty-eight chaperones, cochaperones, or quality-control factors tagged with either 3xFLAG tag or *Renilla* luciferase were stably expressed in 293T cells. Interactors were identified by either AP-MS (3xFLAG tagged proteins) or LUMIER assay (*Renilla*-tagged proteins).

(B) Chaperones, cochaperones, protein quality-control factors, and other proteins characterized in this study.

See also Figure S1.

RESULTS

To systematically characterize the cytoplasmic proteostasis network in human cells, we generated two sets of stable 293T cell lines. One set consisted of 54 proteins tagged with a 3xFLAG-V5 epitope for affinity purification coupled to MS (AP-MS), and the other consisted of 60 proteins fused to *Renilla* luciferase for a quantitative LUMIER assay (Taipale et al., 2012; Figure 1A). Importantly, almost all surveyed proteins were tagged in the C terminus. This ensured that the interactions represent steady-state, posttranslational chaperone-client interactions rather than transient cotranslational interactions (as nascent chains cannot be captured with a C-terminal tag).

We selected proteins for our analysis based on multiple criteria (Figure 1B). First, we cloned all previously identified and characterized Hsp90 cochaperones and Hsp70 nucleotide-exchange factors. Second, we cloned a group of proteins with either a tetratricopeptide repeat (TPR) domain or a CS (CHORD and Sgt1) domain, as most Hsp90 cochaperones contain one or more of these domains (Taipale et al., 2010). Third, we selected several other proteostasis regulators, including four subunits of the 19S proteasome regulatory particle, two subunits of the prefoldin complex, and six HSF family transcription factors. Finally, during the course of the project we identified eight prominent cochaperone interactors, which were cloned for systematic analysis (Figure 1B).

Unbiased Discovery of Chaperone-Cochaperone-Client Interactions by AP-MS

Cochaperones were affinity purified from cell lysates with anti-FLAG beads and interacting proteins identified by MS. To distinguish significant interactors from background noise, we used the SAINTexpress algorithm (Teo et al., 2014). To validate the AP-MS interactions with an orthogonal method, we used the LUMIER assay. In this assay, a prey protein fused to *Renilla* luciferase is stably expressed in 293T cells. Putative interactors (baits) are tagged with a 3xFLAG epitope and transfected into the reporter cell line. Cells lysates are then incubated on 384-well plates coated with an anti-FLAG antibody, leading to capture of the bait protein. Interaction of the bait protein with the tested chaperone can then be quantified as luminescence (Barrios-Rodiles et al., 2005). As a cutoff for high-confidence interactions, we used a LUMIER score ≥ 7 (with an estimated upper bound for false-discovery rate [FDR] of 4.4%).

To characterize the validation rate of AP-MS interactions, we cloned 423 interacting proteins that scored SAINT AvgP ≥ 0.5 in any one of the AP-MS experiments. We tested these proteins for interaction with all 54 baits using LUMIER. Using a stringent cutoff for SAINT (AvgP ≥ 0.85; estimated FDR of 1.8%), 28% of interactions identified in AP-MS were validated by LUMIER, and 81% of them were novel (Figures S1A and S1B available online; Table S1). Conversely, 35% of interactions that scored positive in LUMIER had an AvgP score ≥ 0.85 (Figure S1C). These validation rates are consistent with the observation that any one protein-protein interaction assay can detect about one-third of all interactions without compromising specificity (Braun et al., 2009).

Both the validation rate and the overlap with published interactions decreased with lower scores, supporting our selection of a stringent cutoff (Figures S1A–S1C). We also validated that SAINTexpress was the best computational algorithm for identifying high-confidence interactors in our data set (Figure S1E). Finally, to investigate whether the location of the epitope tag affected the interactions identified, we assayed several proteins again with a tag in the other terminus. The results were highly similar (Figures S2A–S2C).

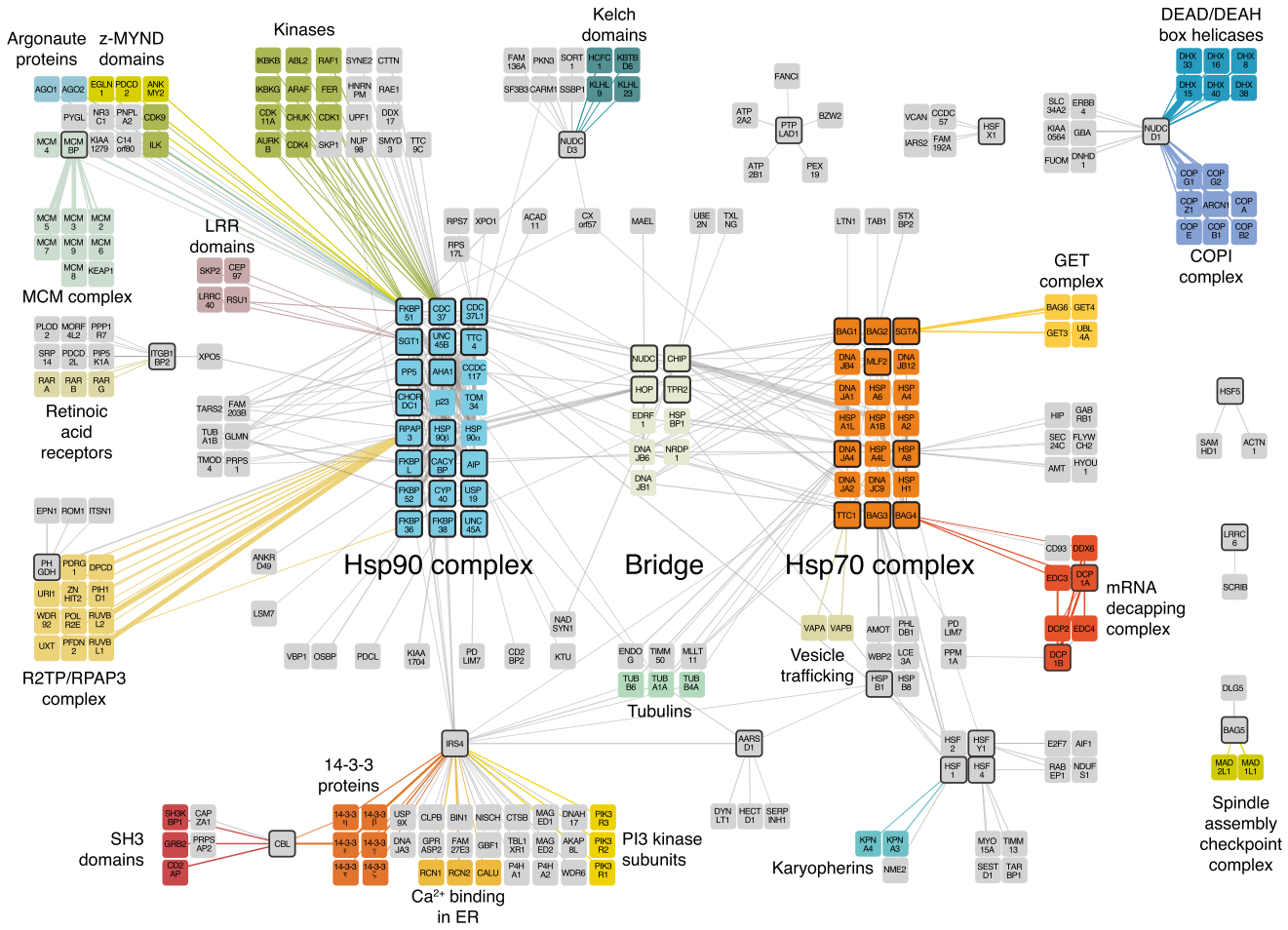

Figure 2. The Proteostasis Network in Human Cells Characterized by MS

Protein-protein interactions were identified by AP-MS and filtered using the SAINTexpress algorithm with cutoff AvgP ≥ 0.85. Proteins are shown as rectangles, and lines represent interactions between the proteins. Bait proteins are indicated by dark edges. The width of the edges corresponds to the number of spectral counts identified for each interaction. Examples of biologically coherent interactions are indicated in colors. See also Figures S1 and S2 and Table S1.

Global Features of the AP-MS Interaction Network: Chaperone Complexes

We identified 486 high-confidence interactions for the 54 tagged baits by AP-MS. The number of identified interactions did not correlate with bait protein expression level, suggesting that no systematic biases were introduced by exogenous expression (Figure S1E). Notably, our chaperone-focused AP-MS network was much larger and more interconnected than chaperone interaction networks that could be recovered from previous large-scale studies (Figures S1F, S2D, and S2E).

The AP-MS network revealed two tiers of organization. The first tier connected all but six bait proteins into a central network with multiple edges between chaperones and their clients (Figure 2). Two subnetworks emerged within this central network, corresponding to known Hsp90 and Hsp70 chaperone complexes (Figure 2, blue and orange squares, respectively). These two subnetworks were bridged by a unique set of cochaperones (Figure 2, tan squares). Among these were the well-known bridging factors HOP/STIP1, TPR2/DNAJC7, and CHIP/STUB1, validating our approach (Brychzy et al., 2003; Schmid et al., 2012; Xu et al., 2002). Other bridging factors in this first tier of organization included members of the Hsp40 chaperone family (DNAJB1 and DNAJB6), HSP70-binding protein 1 (HSPBP1), the TPR domain protein EDRF1, and the E3 ligase NRDP1/RNF41.

Local Features of the AP-MS Interaction Network: Unique Chaperone-Client Interactions

The second tier of organization consisted of cochaperone-client interactions. For example, we identified several protein kinases that copurified with CDC37, a known kinase-specific Hsp90 cochaperone (Taipale et al., 2012). CDC37L1/Harc, a protein that is 62% similar to CDC37 (Figure S3A; Scholz et al., 2001), similarly interacted very strongly with Hsp90 and several of its cochaperones (Figures 2 and 3B). Otherwise, however, the interactions of these cochaperones were unique. For example, CDC37L1 interacted with the bridging factor HOP, whereas CDC37 copurified with AHA1 (Figure 3B), but even more

strikingly, CDC37L1 did not associate with any kinases in AP-MS (Figures 2 and 3B). CDC37L1 lacks the very N terminus of CDC37, which is required for kinase interaction and the cellular function of CDC37 (Shao et al., 2003), and is able to mediate strong interaction with ARAF when fused to CDC37L1 (Figure S3B). Thus, our findings establish that CDC37L1 has evolved a unique position in the Hsp90 chaperone machinery, and that due to its divergent N terminus, CDC37L1 does not associate with kinase clients.

Unique Associations of FKBP Family Cochaperones

Many Hsp90 cochaperones are members of multiprotein families and share significant homology with each other. One of the most prominent of these cochaperone groups is the FK506-binding protein family, or FKBPs. These proteins share an FK506-binding domain and one or more TPR domains, which confer interaction with Hsp90 (Figure 3A). Our AP-MS data set robustly detected shared interactions between these cochaperones and several members of the Hsp90 chaperone machinery (Figure 3B), but it also revealed distinct associations for each.

FKBP51 (aka FKBP5), but none of the other FKBPs, associated with four distinct protein families, pointing to an unexpectedly diverse repertoire of clients. First, FKBP51 interacted with a subset of the kinases that interacted with CDC37 (Figure 3B). Second, FKBP51 interacted with the Argonaute proteins AGO1 and AGO2, which are known Hsp90 clients involved in small RNA biogenesis (Iwasaki et al., 2010). Third, FKBP51 associated with three transcription factors (EGLN1, PDCD2, ANKMY2), all of which contain an MYND zinc finger domain, suggesting that this domain represents an Hsp90-interacting protein fold.

Perhaps most surprisingly, we found that FKBP51 interacted with MCM4 and MCMBP (Figure 3B), two subunits of the MCM complex that are involved in DNA replication initiation and fork progression. FKBP51 purification recovered the most peptides for one particular subunit of the complex, MCMBP (Jagannathan et al., 2012). We validated this interaction by AP of 3xFLAG-tagged MCMBP. Indeed, MCMBP interacted with all members of the MCM complex and with FKBP51 (Figure S3C). Hsp90, however, was not enriched in the MCMBP purifications, and we did not detect an interaction between Hsp90 and MCMBP by LUMIER assay or by coimmunoprecipitation (Figures S3D and S3E), suggesting that FKBP51 associates with MCMBP independently of Hsp90. Thus, our results reveal an unexpected Hsp90-independent link between FKBP51 and genome maintenance. Corroborating our results, a recent systematic small interfering RNA (siRNA) screen identified FKBP51 as a factor in modulating the cellular response to DNA damage (Cotta-Ramusino et al., 2011).

Although their interactomes were significantly more compact than that of FKBP51, all of the other FKBPs also exhibited unique interactions with other proteins (Figure 3B). For example, the FKBP38 (aka FKBP8) interactome suggested a link to G protein signaling through interaction with PDCL, which acts as a chaperone for G protein γ subunits (Lukov et al., 2006; Figure 3B). In contrast, the highly homologous cochaperone FKBP36 (aka FKBP6) did not interact with PDCL, but instead associated with the oxysterol-binding protein OSBP (Burgett et al., 2011; Figure 3B).

FKBP36 as a Sensor for Drug-Target Interactions

We recently reported that Hsp90 and Hsp70 can be used as sensors for drug-target interactions in living cells (Taipale et al., 2013) because they are exquisitely sensitive to the conformational status of the client protein. Binding of a small molecule conformationally stabilizes the protein it targets, decreasing the association of the target with chaperones. Recently, a class of natural products (ORPphilins) with potent activity against cancer cell lines was shown to target OSBP (Burgett et al., 2011). Discovering the OSBP-FKBP36 interaction by AP-MS gave us an opportunity to investigate the general applicability of the chaperone assay for new types of drug-target interactions.

We therefore asked whether the ORPphilin OSW-1 would disrupt the interaction between FKBP36 and OSBP, as measured by LUMIER. Indeed, OSW-1 treatment led to the dissociation of OSBP from FKBP36 (Figure 3C). The potency of OSW-1 in disrupting the interaction was 60 nM (EC_{50}), which is very close to the K_i of the compound (26 nM; Burgett et al., 2011). Next, we tested four structural analogs of OSW-1. Two of them (compounds 6 and 7) are active in cellular assays, whereas compounds 9 and 10 are inactive (Figure S3F; Burgett et al., 2011). Consistent with their different cellular effects, compounds 9 and 10 did not disrupt the OSBP-FKBP36 interaction, whereas compounds 6 and 7 did (Figure 3C). Thus, the biological activity of the OSW-1 family compounds is reflected in their ability to disrupt the interaction between OSBP and FKBP36. Disruption of the interaction could be caused either by overlapping binding sites for FKBP36 and OSW-1 or by thermodynamic stabilization of the OSBP fold. In any case, the use of chaperones and cochaperones as sensors of drug-target interactions is likely to be very broadly applicable.

Unique Associations of BAG Family Cochaperones

BAG proteins comprise a family of homologous cochaperones for Hsp70. All of these proteins regulate Hsp70's ATPase activity, interacting with Hsp70 through a conserved BAG domain in their C termini (Figure 3D; Kampinga and Craig, 2010). Little is known, however, about their biological functions and whether they contribute to Hsp70 client specificity. Again, our AP-MS results pointed to unique biological connections for at least four of the five family members (Figure 3E).

BAG1 interacted with the E3 ubiquitin ligase Listerin (LTN1), which is involved in ribosomal quality control (RQC) of stalled polypeptides (Bengtson and Joazeiro, 2010). As BAG1 is known to regulate the degradation of at least some Hsp70 and Hsp90 clients (Tsukahara and Maru, 2010), our results suggest it may be also involved in the degradation of proteins targeted by RQC. As previously reported (Fuchs et al., 2010), BAG3 associated with the small heat shock proteins Hsp22/HSPB8 and Hsp27/HSPB1. In addition, we detected a robust interaction with HSF1, the master regulator of the heat-shock response (Figure 3E).

BAG5 and BAG4 interacted with protein complexes that have not previously been associated with chaperones. BAG5 purification revealed the spindle checkpoint components Mad1/MAD1L1 and Mad2/MAD2L1 as the most prominent interactors (Schuyler et al., 2012). BAG4, in contrast, interacted with three

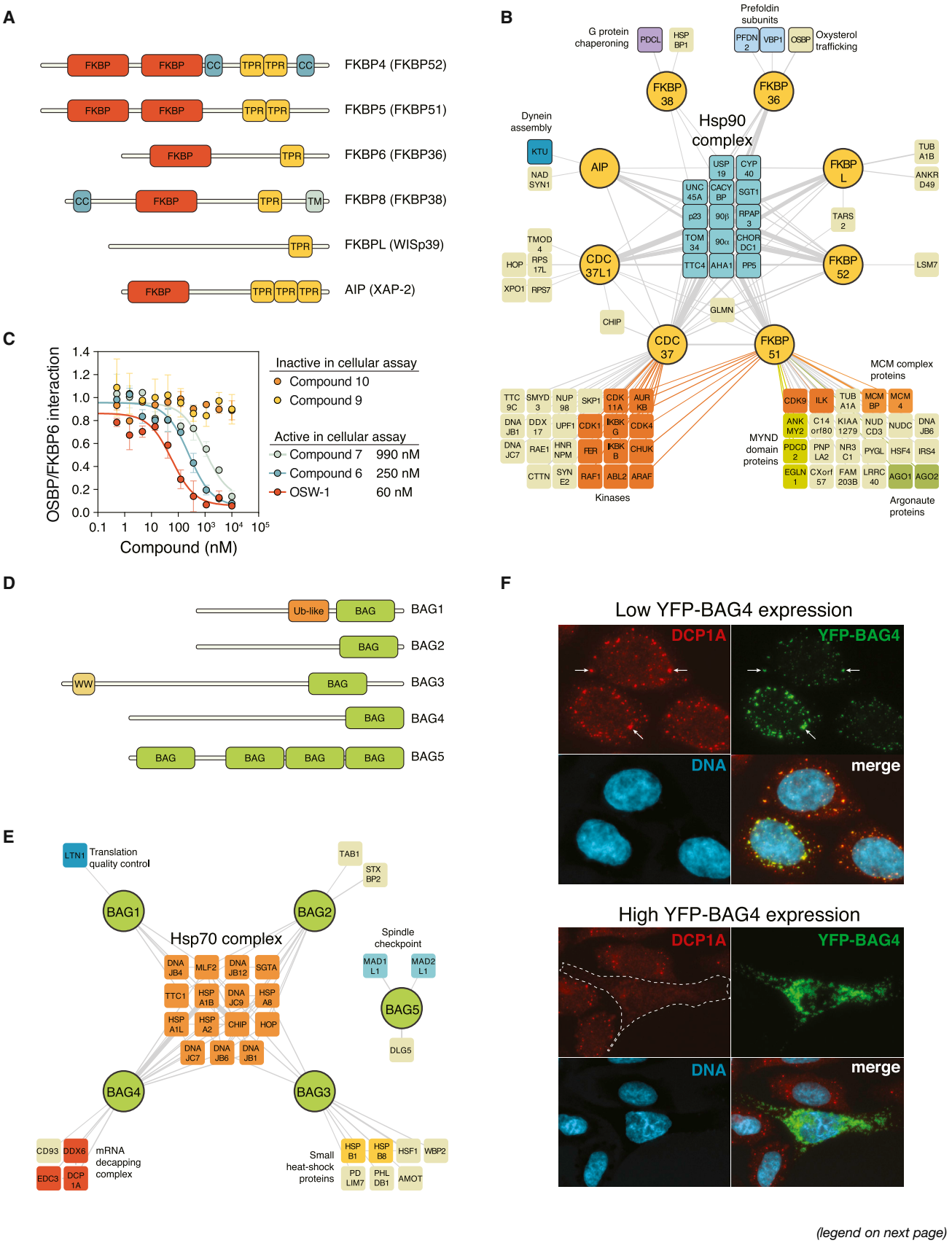

(legend on next page)

central components of the mRNA decapping complex: DCP1A, EDC3, and DDX6 (Figure 3E). These three proteins localize to cytoplasmic structures known as processing bodies, or P bodies, which are involved in mRNA decapping, degradation, and translational silencing (Eulalio et al., 2007).

To test whether BAG4 also localizes to P bodies, we transfected HeLa cells with EYFP-BAG4. When EYFP-BAG4 was expressed at low levels, it colocalized with endogenous DCP1A in cytoplasmic foci (Figure 3F). Because overexpression of P body components often modulates P body formation (Eulalio et al., 2007), we also examined cells in which BAG4 was expressed at high levels. In such cells, EYFP-BAG4 was localized more diffusely in the cytoplasm and DCP1A localization also became diffuse (Figure 3F, lower panel). Thus, BAG4 overexpression disrupted P body organization. We then investigated whether this effect was dependent on the association of BAG4 with Hsp70. We introduced a point mutation in the BAG domain of BAG4 (D424A) that disrupts its association with Hsp70 (Briknarová et al., 2002; Figure S3G). However, mutant BAG4 still localized to P bodies and disrupted P body organization at high expression levels (Figure S3H). Our data thus establish BAG4 as a component of P bodies and suggest that this function is independent of Hsp70.

Quantitative Profiling of the Human Chaperone-Client Landscape

The network we uncovered by AP-MS was surprisingly compact and likely represented only the most abundant chaperone-client interactions. To further expand the network and to investigate more quantitatively how client proteins are integrated within it, we systematically surveyed pairwise interactions between clients and cochaperones with LUMIER. To this end, we constructed a panel of 800 query proteins (Table S1). This set included known Hsp90 clients (http://www.picard.ch), a subset of kinases, E3 ligases and transcription factors that we previously identified as Hsp90 clients (Taipale et al., 2012), and the 423 proteins that we used to characterize the overlap between AP-MS interactors and LUMIER assay (see above). After we filtered out proteins that were not expressed at detectable levels, our data set comprised 40,604 pairwise assays, each performed in duplicate.

We first examined the effects of the Hsp90 inhibitor ganetespib on Hsp90 and Hsp70 interactions (Ying et al., 2012). This served two purposes. First, Hsp90 inhibition leads to dissociation of most known clients from Hsp90 (Taipale et al., 2012). Although dissociation does not directly prove that the interactor is a client, it provides supportive evidence. Second, this allowed us to test the generality of client handoff from Hsp70 to Hsp90. Previous studies have shown that Hsp90 inhibition is accompanied by accumulation of clients with the upstream chaperone Hsp70 (Xu et al., 2002). Our platform enabled us systematically test this model. To this end, cells expressing *Renilla* tagged Hsp90β or Hsc70 were transfected with the bait protein collection and treated with 1 μM ganetespib for 1 hr before LUMIER assay.

Ganetespib treatment had a strong effect on most Hsp90-client interactions. Of the 630 unique proteins that we detected by LUMIER assay, 46% significantly decreased their interaction with Hsp90β (change in LUMIER score > 1.5, adjusted p value < 0.05; Figure 4A). Using a binary cutoff for Hsp90β interactions (LUMIER score $\geq$ 7), 81% of high-confidence interactors (84/104) decreased their interaction with the chaperone (Table S1). Notably, one-third (7/20) of those that still interacted with Hsp90β were known cochaperones (Figure 4A; Table S1). Yet, even some cochaperones lost their interaction with Hsp90. This is consistent with the observation that Hsp90 inhibitors stabilize a specific conformation of the chaperone, leading to differential cochaperone interactions (Gano and Simon, 2010). The effect of ganetespib on Hsc70 interactions was more subtle but still clearly detectable: 16% of the tested proteins increased their interaction with Hsc70 upon ganetespib treatment. This was particularly noticeable for proteins that interacted strongly with Hsc70 (Figure 4B). None of the tested Hsp70 cochaperones were affected by inhibitor treatment (Figure 4B).

We then compared the effects of ganetespib on Hsp90β and Hsc70 interactions (Figure 4C). Most proteins that decreased their association with Hsp90β did not significantly change their interaction with Hsc70. Those that did, however, generally associated more strongly with Hsc70 (red circles, Figure 4C). This group of proteins was enriched in kinases ($p < 0.0001$, Fisher's exact test; Table S1). A few, mostly cochaperones, decreased their interaction with both Hsp90β and Hsc70 (blue circles, Figure 4C). Interestingly, five proteins increased their interaction with both Hsp90 and Hsp70 after drug treatment (orange circles, Figure 4C). They might represent clients that are chaperoned in a distinct manner.

Taken together, these experiments demonstrate that Hsp90 inhibition leads to an almost global loss of Hsp90-client interactions. This is accompanied by a more subtle increase in Hsp70 interaction for many clients, in particular kinases. The results also suggest that the vast majority of these interactions are true chaperone-client interactions.

Figure 3. Unique Associations of FKBP and BAG Family Cochaperones

(A) The FKBP (FK506-binding protein) family of Hsp90 cochaperones is characterized by one or more TPR domains that can interact with Hsp90 and the FKBP domain.

(B) Interaction network of FKBP family cochaperones. Selected unique interaction partners and protein classes are indicated.

(C) The natural compound OSW-1 disrupts the interaction between OSBP and FKBP36. 3xFLAG-tagged OSBP was transfected into 293T cells stably expressing FKBP36-Renilla luciferase fusion. One hour before cell lysis, cells were treated with a dilution series of the indicated compounds. The interaction between OSBP and FKBP36 was then measured with LUMIER. Error bars indicate SD.

(D) BAG proteins are a family of homologous Hsp70 cofactors that interact with Hsp70 through their BAG domain.

(E) Interaction network of BAG family cochaperones. Selected unique interaction partners are indicated.

(F) BAG4 colocalizes with the P body component DCP1A and regulates P body assembly. Top panel: YFP-BAG4 (green) was transfected into HeLa cells, which were then fixed and stained for endogenous DCP1A (red), a component of P bodies. DNA was stained with Hoechst 33342 (cyan). Bottom panel: in cells where YFP-BAG4 is expressed at high levels, endogenous DCP1A appears diffuse.

See also Figure S3.

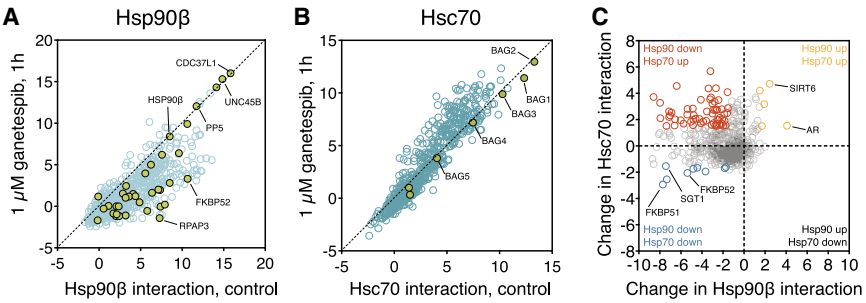

Figure 4. Effect of Transient Hsp90 Inhibition on Chaperone Interactions

(A) Hsp90 inhibition leads to dissociation of most clients from Hsp90β. Hsp90β was surveyed for interaction with 800 proteins by LUMIER assay. Cells were treated for 1 hr with 1 μM ganetespib or left untreated before the assay. Hsp90 cochaperones are shown as green circles. Interaction strength was quantitated as LUMIER scores.

(B) Hsp90 inhibition leads to stronger association of some proteins with Hsc70. Hsc70 was assayed for interaction with 800 proteins as in (A). Hsp70 cochaperones are shown as green circles.

(C) Comparison of the effects of ganetespib on Hsp90β and Hsc70 interactions. The plot shows the change in interaction of 800 tested proteins with Hsp90β and Hsc70 (change is defined as LUMIER score drug – LUMIER score control). Proteins that show differential association with both chaperones are indicated in orange (both increase), blue (both decrease), or red (decrease in Hsp90β interaction, increase in Hsc70 interaction). Selected proteins are labeled.

See also Table S1.

Unbiased Clustering of Proteostasis Regulators by Protein Interaction Profiles

The application of quantitative analyses has often revealed unexpected associations between genes in gene-expression and genetic-interaction profiles (Eisen et al., 1998; Tong et al., 2004). The quantitative readout of our assay allowed us to exploit this approach for the analysis of protein-protein interactions. That is, rather than employing statistical cutoffs to determine significant interactions, we used the entire data set and treated interaction scores as quantitative variables. Although LUMIER scores do not directly correspond to biophysical parameters such as affinity or stoichiometry, correlations in the interaction profiles can reveal novel relationships between proteins.

We first clustered chaperones and cochaperones based on their similarities in client-interaction profiles. This recovered well-known biological complexes (Figure 5A). For example, Hsp70 and Hsp90 machineries formed distinct clusters: Hsp70 clustered together with Hsc70, their nucleotide-exchange factor BAG2, and the E3 ligase CHIP (Figure 5A, orange cluster), whereas Hsp90 and many of its cochaperones formed a separate group (Figure 5A, blue cluster). Similarly, three components of the proteasome regulatory particle (PSMD4, PSMC1, and ADRM1) clustered together, as did the two subunits of the prefoldin complex, PFDN2 and PFDN5 (Figure 5A). Notably, some of the clusters formed by LUMIER interactions were different from those recovered in AP-MS. RPAP3 interacted strongly with the Hsp90 machinery in AP-MS, but its interaction profile in LUMIER connected it more tightly with prefoldin subunits. The most likely explanation for this is that chaperone complexes in AP-MS are mainly connected by interactions between complex members, whereas LUMIER clusters tend to be determined by shared interactions of cluster members. The recovery of well-established, biologically coherent chaperone clusters interacting with a diversity of known substrate proteins validates our approach.

Paralogous Chaperones Have Very Similar Client and Cochaperone Interactions

We first examined the interaction profiles of the Hsp90 and Hsp70 family chaperones. As expected, cochaperones showed distinct specificities for Hsp90 (Figure 5B, red circles) or Hsp70 (Figure 5B, ochre circles). However, most clients interacted with both Hsp90β and Hsc70 to a similar degree (Figure 5B, light blue circles). Consequently, the interaction profiles of the chaperones were themselves correlated (R^2 = 0.34). Yet, some clients clearly preferred one chaperone over the other. Hsp90β interacted particularly strongly with kinases (Figure 5B, filled blue circles), whereas the transcription factors p53 and HSF1 were among the most Hsp70-biased interactors (Figure 5B, green circles).

We then compared the interaction profiles of different Hsp70 and Hsp90 isoforms. Virtually all eukaryotic genomes encode multiple isoforms of both of these chaperones, even within the same cellular compartment (Powers and Balch, 2013). However, it is not known whether they have distinct client-protein preferences. The three cytoplasmic Hsp70 isoforms we profiled (Hsp70, Hsc70, and Hsp70B′) had very similar interaction profiles across the 800 proteins we tested (Figures 5C and S4B). Similarly, the interaction profiles for Hsp90α and Hsp90β correlated strongly (R^2 = 0.76; Figure 5D). A few cochaperones had strong isoform preferences. BAG proteins interacted more strongly with Hsp70B′ than with Hsp70 or Hsc70 (Figure S4B and data not shown). The Hsp90 cochaperone UNC45A, but not its homolog UNC45B, were previously described as an Hsp90β-specific cochaperone (Chadli et al., 2008) and this held true in our assay. We detected a similar preference for FKBP38 (Figure 5D). We further validated the isoform preference of UNC45A and FKBP38 by coimmunoprecipitation with the endogenous Hsp90 isoforms (Figure S4A). These outliers provide an avenue for investigating distinctions in the functions of specific chaperone isoforms. By and large, however, Hsp70 and Hsp90 isoforms interacted with the same clients and cochaperones, and did so with very similar affinities.

BAG2 and RPN1 Are Tightly Connected to the Hsp70 Machinery

Our AP-MS interaction network suggested unique roles for each of the BAG proteins, except for BAG2 (Figure 3E). Illustrating the power of combining unbiased AP-MS analysis with the quantitative nature of the LUMIER assay, we uncovered a striking interaction pattern for BAG2. Across the 800 queried proteins, BAG2 interactions were remarkably similar to those of Hsc70 (R^2 = 0.77; Figure 5E). In contrast, the other BAG proteins had

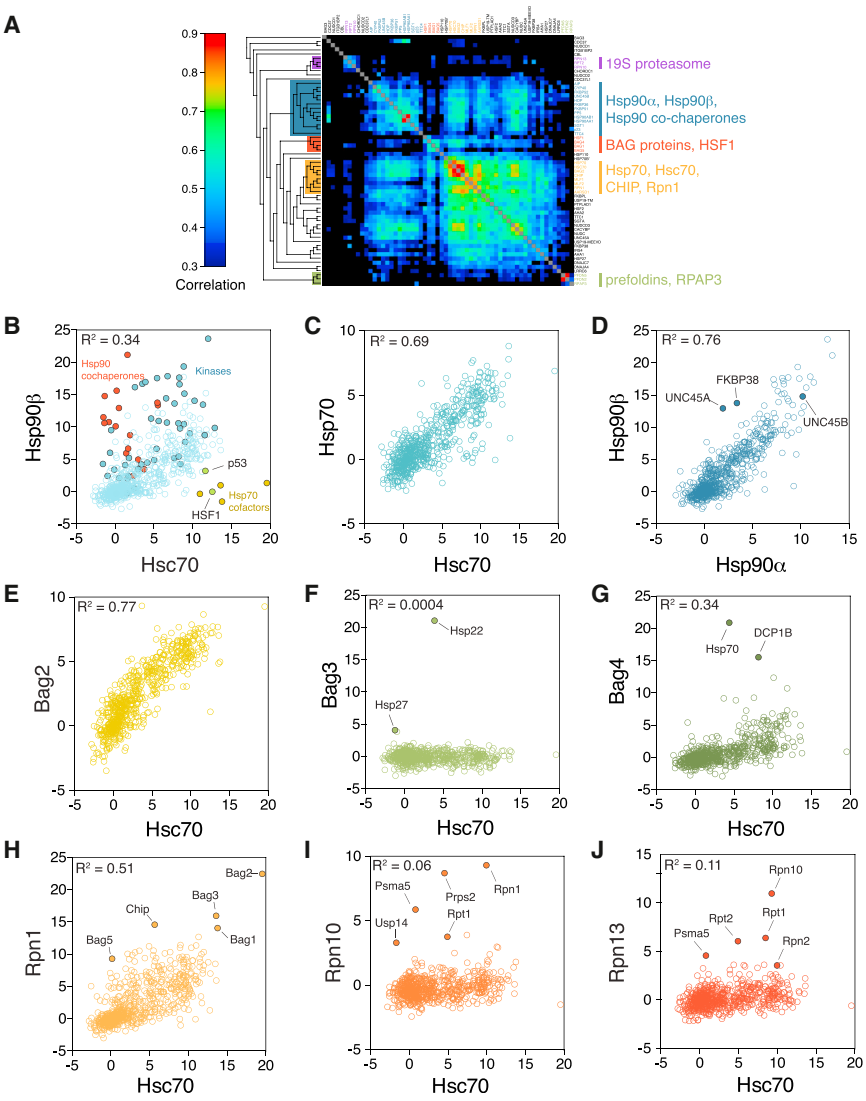

Figure 5. Clustering of Chaperones, Cochaperones, and Quality-Control Factors Based on Similarities in Client Interaction Profiles

(A) Chaperones, cochaperones, and protein quality-control factors were clustered based on their interaction profiles with 800 query proteins. Clustering corresponds well to known biological complexes. Three components of the 19S proteasome (purple) cluster together, as do two prefoldin subunits (green). Hsp70 and its cofactors (yellow) and BAG proteins (red) cluster separately from Hsp90 and its cochaperones (blue).

(B) Significant correlation between Hsc70 and Hsp90 client interaction profiles. A total of 800 proteins (light blue) were assayed for interaction with Hsc70 or Hsp90 by LUMIER. Hsp90 cochaperones (red) interact exclusively with Hsp90, and Hsp70 cochaperones (ochre) interact exclusively with Hsc70. Kinases (filled blue circles) generally interact more strongly with Hsp90 than with Hsc70, whereas p53 and HSF1 (green) prefer Hsc70.

(C) The client interaction profiles of Hsp70 isoforms Hsc70 and Hsp70 are highly similar.

(D) The client interaction profiles of Hsp90 isoforms Hsp90α and Hsp90β are highly similar. Most clients (blue) interact with Hsp90α and Hsp90β to a similar degree. The cochaperones UNC45A and FKBP38 (filled blue circles) interact more strongly with Hsp90β. In contrast, the UNC45A paralog UNC45B interacts with both isoforms to a similar degree.

(E) The BAG2 interaction profile is almost identical to that of Hsc70, suggesting that it is a general cofactor for Hsp70 chaperones. In contrast, BAG3 (F) and BAG4 (G) are more specific, interacting primarily with the small heat shock proteins Hsp22 and Hsp27 (BAG3) and the mRNA decapping factor DCP1B (BAG4)

(H–J) Rpn1 (H) is a component of the proteasome regulatory particle and its interaction profile correlates significantly with that of Hsc70. In contrast, Rpn10 (I) and Rpn13 (J), also components of the core particle, mainly interact with other subunits of the proteasome.

See also Figure S4.

highly specific interactions that complemented our results from AP-MS. BAG3 and BAG4 showed a strong association only with the small heat shock protein Hsp27 (Figure 5F) and the mRNA decapping complex member DCP1B, respectively (Figure 5G), whereas BAG1 interacted with several proteasome subunits (Figure S4C). Thus, BAG2 appears to be a general cofactor for Hsp70 with little client protein preference, whereas other BAG proteins have unique clients.

The interaction profile of RPN1/PSMD2, a subunit of the proteasome regulatory particle, was also highly correlated with that of Hsc70 (R^2 = 0.51; Figure 5H). RPN1 interacted strongly with four BAG proteins and with the ubiquitin ligase CHIP. This was in contrast to the three other subunits (RPN10, RPN13, and RPT2) that primarily interacted with other proteasome subunits (Figures 5I, 5J, and S4E). Although all four subunits are part of the base of the proteasome regulatory particle (Lander et al., 2012), RPN1 clustered together with Hsp70 rather than with the other proteasome subunits (Figure 5A). RPN1 is thought to act as a scaffold protein that binds and recruits diverse proteasome-associated factors to the proteasome (Finley, 2009). The correlation between the RPN1 and Hsc70 interaction profiles suggests that RPN1 could also serve as a bridge between protein folding by the Hsp70 machinery and protein degradation by the proteasome.

Another factor that correlated well with Hsc70 was the ubiquitin ligase CHIP (Figure S4E). CHIP binds Hsp90 and Hsp70 with similar affinities and can regulate the degradation of chaperone clients (Kundrat and Regan, 2010). However, LUMIER revealed an interaction profile that correlated with Hsc70 (R^2 = 0.74) even more strongly than with Hsp90β (R^2 = 0.38; Figures S4F and S4G). Indeed, hierarchical clustering placed it together with Hsp70 proteins rather than with Hsp90 (Figure 5A). This finding suggests that CHIP is most tightly coupled to the Hsp70 chaperone machinery.

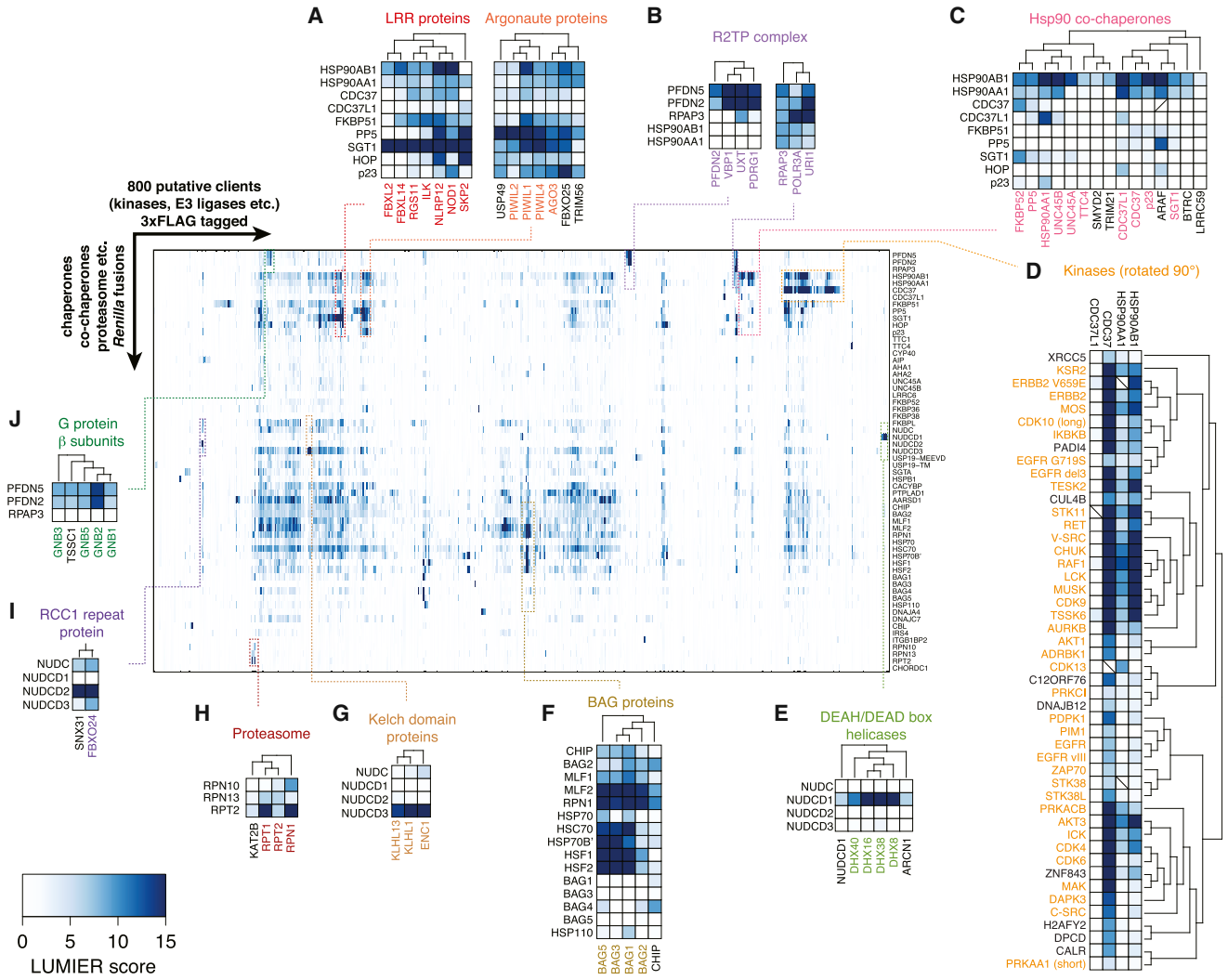

Figure 6. Quantitative View of the Human Protein-Folding Landscape

A total of 800 query proteins (arranged in columns) were assayed for interaction with 60 different chaperones, cochaperones, and quality-control factors (rows) by a quantitative LUMIER assay. Query proteins were clustered based on their interaction profiles. Some of the biologically coherent clusters are highlighted in more detail. Proteins that share the same fold or are part of the same biological complex in each cluster are indicated in color.

(A) LRR proteins (red) and Argonaute proteins (orange) form distinct clusters. LRR proteins interact strongly with SGT1, while Argonaute proteins associate with PP5.

(B) The R2TP complex members (purple) form two separate clusters.

(C) Hsp90 cochaperone cluster.

(D) Kinases (orange) cluster together and interact specifically with CDC37, but not with CDC37L1.

(E) NUDCD1 associates with DEAH/DEAD box helicases (green).

(F) BAG proteins that cluster together interact strongly with Hsp70 proteins, Rpn1, Hsf1, and Hsf2.

(G) Kelch domain protein cluster (brown) with NUDCD3.

(H) Proteasome cluster.

(I) RCC1 repeat protein FBXO24 (purple) interacts with NUDCD2.

(J) G protein γ subunits (green) interact with prefoldins.

See also Table S1.

Quantitative Client Profiling Reveals Unique Cochaperone Specificities

We next focused on the client specificity of chaperones and cochaperones, and clustered the 800 tested clients based on their LUMIER interaction patterns. This analysis revealed several client groups that shared specific chaperones or cochaperones (Figure 6). For example, seven members of the cytoplasmic RNA polymerase assembly complex R2TP interacted with the prefoldin subunits PFDN2 and PFDN5. However, the R2TP subunits formed two distinct clusters (Figure 6B). The four proteins in

the first cluster (PFDN2 itself, VBP1, UXT, and PDRG1) are all prefoldin-like proteins and interacted primarily with PFDN2 and PFDN5. The second cluster (URI1, POLR3A, and RPAP3) interacted also with RPAP3 and Hsp90 in addition to the prefoldins (Figure 6B). Yet another distinct prefoldin interaction module consisted of G protein β subunits, linking prefoldins to G protein-coupled receptor (GPCR) signaling (Figure 6J). While prefoldins generally have been thought to participate primarily in the folding of actin and tubulin (Lundin et al., 2010), our results expand the specificity of this little-characterized chaperone system.

Hierarchical clustering of the LUMIER data revealed several additional cochaperone modules. Proteins with kinase domains clustered together, as was expected from their known preference for CDC37 (Figure 6D). Leucine-rich repeat (LRR) proteins and Argonaute proteins also formed distinct clusters. LRR proteins interacted particularly strongly with the SGT1 cochaperone, whereas Argonaute proteins bound the protein phosphatase PP5 and p23, both of which are well-characterized Hsp90 cochaperones (Figure 6A).

NUDC Family Cochaperones Associate with Distinct β-Propeller Folds

Perhaps the most striking client specificity we uncovered by LUMIER involved the NUDC family of cochaperones. The human genome encodes four evolutionarily related proteins in this family (Figure S5A). NUDC proteins have been found to associate with the Hsp90 complex, but the biological roles of these cochaperones are largely unknown (Zheng et al., 2011).

We noticed that three of the four NUDC proteins associated with a group of proteins that had no functional relationship to each other, yet contained structurally related folds. NUDC interacted strongly with WD40 repeat proteins (Table S1). NUDCD3, in contrast, interacted with proteins with Kelch domains (Figure 6G; Table S1). For NUDCD2, the most significant interacting protein was FBXO24, an RCC1 repeat protein (Figure 6I). Since WD40, Kelch, and RCC1 domains all have β-propeller folds, we reasoned that NUDC proteins might represent a novel family of β-propeller specific cochaperones.

To more rigorously test the specificity of NUDC proteins, we cloned into our LUMIER vector 275 genes that contained a predicted β-propeller domain. In addition, we cloned 156 genes with LRRs, because several LRR proteins clustered together as SGT1-interacting clients (Figure 6A). Finally, we included as controls 80 kinases that were strong Hsp90 and Cdc37 clients (Taipale et al., 2012). We quantitatively assayed the interaction of these 511 proteins with SGT1, CDC37, and all four NUDC family members (Figure 7A). Except for NUDCD1, each cochaperone showed a striking client preference. As expected, CDC37 interacted virtually exclusively with kinases ($p < 0.0001$, Mann-Whitney test; Figure 7A). Similarly, although SGT1 interacted with some non-LRR proteins, it had significantly stronger interactions with LRR proteins than with other domains ($p < 0.0001$). NUDC selectively associated with WD40 repeats, NUDCD2 with RCC1 repeats, and NUDCD3 with Kelch domains ($p < 0.0001$ for each; Figure 7A). Although there was additional weak crosstalk between some of these cochaperones and their clients, these specific associations stood out. We further validated the specificity of NUDC and NUDCD3 with AP-MS. Endogenous NUDC, but not NUDCD3, copurified with the 3xFLAG-tagged WD40 protein FBXW2, whereas endogenous NUDCD3, but not NUDC, copurified with five different 3xFLAG-tagged Kelch domain proteins in 293T cells (Figure S5B).

We then tested whether the cochaperone specifically bound the kinase, β-propeller, or LRR domain by coimmunoprecipitation (Figures 7B and S5A). As reported before (Taipale et al., 2012), CDC37 interacted with the kinase domain of ARAF, and SGT1 interacted with the LRR domain of FBXL2 (Figure 7B). NUDC interacted with the WD40 domain of FBXW2, NUDCD2 interacted with the RCC1 domain of FBXO24, and NUDCD3 interacted with the Kelch domain of KLHL38 (Figure 7B). In each case, the interaction with these isolated domains was as strong as that with the full-length protein. These results establish that the evolutionarily related NUDC cochaperones recognize a specific β-propeller fold in their clients (Figure 7C).

NUDCD1 was the only member of the NUDC family that did not interact with β-propeller domain proteins in our query set. However, AP-MS and LUMIER revealed that it did interact strongly with multiple DEAH/DEAD box RNA helicases and several subunits of the COPI complex, which regulates retrograde signaling between Golgi compartments (Figures 2 and 6E). Although two members of the COPI complex (COP-α and COP-γ2) contain β-propeller domains, we could not detect an interaction between these subunits and NUDCD1 (data not shown). Interestingly, however, in contrast to other NUDC proteins, NUDCD1 itself contains a β-propeller domain (Figures 7C and S5A), which also connects this cochaperone to β-propeller domains.

Cochaperones May Facilitate the Evolutionary Diversification of Protein Folds

We next asked whether the emergence of fold-specific cochaperones might have enabled the diversification of their client protein folds during evolution. Chaperones with broad client specificities can promote evolution by providing a buffering mechanism against destabilizing mutations (Jarosz et al., 2010; Tokuriki and Tawfik, 2009). Domain-specific cochaperones might facilitate evolution in a similar but domain-specific manner. We therefore analyzed the genomes of 147 fully sequenced organisms. We calculated the number of proteins with cochaperone-specific protein folds (LRR, WD40, Kelch, and RCC1) and asked whether the number of such proteins was larger in genomes that contain the specific cochaperone compared with those without the cochaperone (after controlling for nonspecific expansion of the proteome). Genomes that contained the NUDCD3 or SGT1 cochaperones showed a striking and highly significant enrichment for their client folds (Kelch and LRR, respectively; Figures 7D and 7E). The associations of NUDC and NUDCD2 with their cognate client folds were not statistically significant (data not shown). These results suggest that the evolution and diversification of LRR domains and Kelch repeats may have been promoted by the emergence of cochaperones specific to these folds.

DISCUSSION

We have systematically and quantitatively characterized the chaperone-cochaperone-client interactome in human cells.

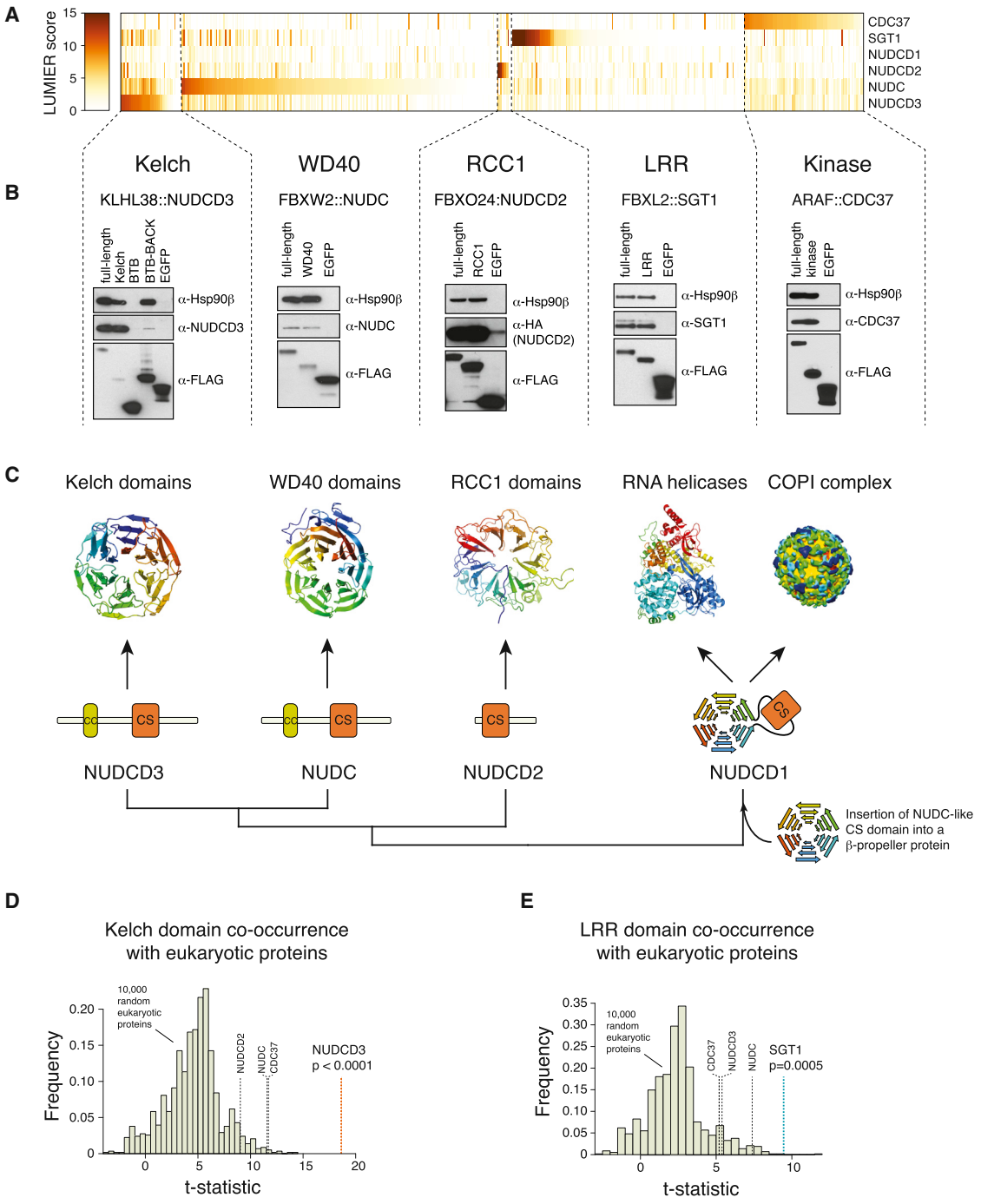

Figure 7. NUDC Family Proteins Are Specific Cochaperones for β-Propeller Domains

(A) NUDC family cochaperones, SGT1, and CDC37 were assayed with a quantitative LUMIER assay for interaction with 80 kinases, 156 LRR domain proteins, and 275 proteins with a β-propeller domain. Bait proteins are organized by domain (annotated below) and rank sorted based on their interaction with a specific cochaperone (kinases with CDC37, LRRs with SGT1, WD40 with NUDC, RCC1 with NUDCD2, and Kelch with NUDCD3).

(B) Cochaperones recognize specific domains in their clients. The indicated full-length proteins or truncated constructs were tagged with a 3xFLAG epitope and transfected into 293T cells. Their interaction with endogenous Hsp90 (top panel) or with endogenous, specific cochaperone (middle panel) was assayed by coimmunoprecipitation. For NUDCD2, a 3xHA-tagged construct was cotransfected with FBXO24 and the blot was probed with an anti-HA antibody.

(C) Evolution of the NUDC protein family members and their client specificity. NUDC, NUDCD2, and NUDCD3 each recognize distinct β-propeller folds. NUDCD1, in contrast, associates with proteins with an unrelated fold (RNA helicases and the COPI complex), but itself contains a β-propeller domain. The COPI complex image is used with permission from *Science Magazine*.

(legend continued on next page)

The broad and quantitative nature of our approach allowed the analysis of protein-protein interaction data by hierarchical clustering, illuminating unexpected and highly specific connections between chaperones and particular biological processes. We validated many interactions by orthogonal interaction assays and functional assays, but, as in any endeavor of this size, a large fraction of the network remains unexplored. Here, we highlight only the most salient insights revealed by our analysis, to encourage others to explore this resource in their own investigations.

Cochaperones and Protein Complex Assembly

Systematic studies of the components of the proteostasis networks have almost exclusively focused on chaperones rather than their cofactors. Our data suggest surprisingly diverse roles for cochaperones in particular cellular processes, including spindle assembly (BAG5 and MAD proteins), DNA replication (FKBP51 and the MCM complex), mRNA decapping (BAG4 and P bodies), and GPCR signaling (prefoldins and G protein β subunits). These cellular processes are completely unrelated, yet conceptually they share key features. The cochaperone interactors are individual components of much larger multiprotein complexes, and in each case these complexes must be assembled in a specific location at a specific time. Further, their assembly is often regulated by dramatic conformational changes in the associated proteins.

Our results suggest that cochaperones are broadly involved in the assembly of multiprotein complexes. On the one hand, cochaperones provide a means of recruiting the Hsp90 or the Hsp70 chaperone system to very specific biological processes. In contrast to Hsp70, which generally recognizes unfolded proteins with exposed hydrophobic stretches, cochaperones associate with proteins that have specific domains. Presumably, they associate with domains that are at least transiently recognizable yet retain a level of conformational flexibility that guides them to the chaperone machinery. Recruitment of Hsp70 by these cochaperones would thus create a local pool of the chaperone to facilitate transitions between conformational states. On the other hand, certain cochaperone interactions are independent of the core chaperones (e.g., FKBP51 and the MCM complex) and likely serve specific roles that do not require extensive structural rearrangements driven by chaperones. It will be of great interest to determine whether those functions evolved from the initial chaperone interaction or vice versa.

Domain-Specific Cochaperones, Client Protein Recognition, and Protein Fold Evolution

Our analysis revealed that in addition to the well-known kinase specificity of CDC37, other cochaperones also have distinct specificities. SGT1 interacts particularly strongly with clients with LRRs. (This was suggested previously [Kadota et al., 2010], but awaited systematic testing.) We also uncovered previously unsuspected specificities for the poorly characterized NUDC family cochaperones. These evolutionarily related cochaperones recognized distinct but structurally homologous β-propeller domains (Figure 7C). The interaction patterns of all of the domain-specific cochaperones were analogous to that of CDC37. That is, although the cochaperones clearly preferred a specific protein fold, neither they nor Hsp90 associated with all members of that family. Furthermore, the clients did not phylogenetically cluster, but were scattered throughout the evolutionary tree (Figure S5C). When they did interact, the strength of the interactions varied over a broad continuum (Figure S5C). Thus, these results point to a dynamic process of evolutionary diversification that is still at work.

In addition to their specific cochaperones, many β-propeller proteins interacted with Hsp90, Hsp70, and prefoldins. WD40 domain proteins have also been shown to associate with the TRiC/CCT chaperonin (Yam et al., 2008). Why might β-propeller domains require so many chaperones and a dedicated system of cochaperones? The canonical β-propeller structure provides a clue. β-propellers are composed of repeating units of four antiparallel β-sheets arranged around a ring. β-sheets from the last repeat are often circularly permuted to the first repeat, closing the ring. We suggest that these proteins have a particularly high requirement for chaperone proteins to keep the β-propeller soluble before ring closure occurs.

β-propellers from different families share very little sequence homology, and therefore it has been difficult to resolve whether they evolved from a common ancestral fold or the fold is an example of convergent evolution (Chaudhuri et al., 2008; Hudson and Cooley, 2008). Our results suggest that common ancestry is the more parsimonious scenario. That is, the evolution of β-propeller folds by duplication and diversification was facilitated by the evolutionary expansion of the NUDC family. This seems more plausible than the alternative scenario, where unrelated repeats happened to converge on the same fold while requiring highly related NUDC chaperones.

Our evolutionary analysis revealed that Kelch and LRR domains coevolved with their cochaperones NUDCD3 and SGT1, respectively. Eukaryotic proteomes with these cochaperones contain a larger fraction of their respective client protein folds compared with proteomes without them. Although it is possible that these cochaperones evolved as a response to an expanded repertoire of client protein folds, we consider it more likely that the emergence of NUDCD3 and SGT1 promoted the divergence of the clients. The finding that chaperones can buffer genetic variation in several model organisms and in experimental evolution supports this interpretation (Jarosz et al., 2010; Tokuriki and Tawfik, 2009).

(D) Genomes that encode the Kelch-domain specific cochaperone NUDCD3 contain significantly more proteins with Kelch domains than genomes without NUDCD3. The number of Kelch domains was analyzed in each of 147 fully sequenced eukaryotic proteomes. Normalized Kelch domain abundance (as a fraction of total number of proteins) was compared between species that have the NUDCD3 ortholog and those that do not. Histograms display the t-statistic distribution for 10,000 random eukaryotic proteins that were assayed for similar evolutionary co-occurrence with Kelch domains. The orange line shows the t-statistic for NUDCD3 and black lines show the t-statistic for three other cochaperones that are not Kelch specific.
(E) Evolutionary analysis of LRR domain evolution with LRR-specific cochaperone SGT1, performed as in (D).
See also Figure S5 and Table S1.

Concluding Remarks

The architecture of the chaperone-cochaperone-client interaction network reported here has broad implications for human biology and medicine. A large number of human diseases, ranging from cystic fibrosis to cancer and neurodegeneration, are now known to ultimately stem from problems in the folding of specific proteins. However, these proteins do not misfold in isolation. Rather, their misfolding ramifies at a system-wide level to impinge on critical cellular functions (Powers et al., 2009), derailing the homeostatic control of protein folding, trafficking, and degradation in a tissue-specific manner. The interaction network we have uncovered provides a robust framework for systematically dissecting the effects of such perturbations and characterizing the unique features of the network in different tissues and cellular states.

In addition, these interactions can be exploited to study drug-target interactions in living cells (Taipale et al., 2013). Here, we further expanded this approach to another cochaperone, FKBP36. It is very likely that many chaperone-client interactions will prove amenable to such an analysis. Furthermore, given that the approach relies on fundamental biophysical principles rather than a specific functional readout, it should be generally applicable to proteins that traditionally have been difficult to assay for small-molecule binding. Thus, our results provide not only a springboard for deciphering how the protein homeostasis network is dynamically rewired in various disease states, but also a platform for evaluating the therapeutic potential of small molecules that could ameliorate such perturbations.

EXPERIMENTAL PROCEDURES

Clones and Cell Lines

All clones originated from the human ORFeome collection 7.1 or were cloned from cDNA by PCR. Clones were transferred into a mammalian expression vector with a 3xFLAG-V5 epitope tag or a pLenti6-based lentiviral vector containing a 3xFLAG-V5 epitope tag or *Renilla* luciferase protein. Stable polyclonal 293T cell lines were established by lentiviral infection, and expression of each protein was verified by western blotting or luciferase assay. Mutant constructs were created by site-directed mutagenesis. All clones used in the study were validated by sequencing or by restriction digestion.

LUMIER Assay

LUMIER assay was performed as previously described (Taipale et al., 2012) with one modification. Instead of calculating the prey/bait (luminescence/ELISA) ratio, we used normalized luminescence Z scores as a quantitative interaction measure. ELISA values were used to remove bait proteins that were not detectably expressed in the assay (see Extended Experimental Procedures for details).

AP-MS

AP-MS was performed as previously described (Kean et al., 2012) except that sodium molybdate was included in the lysis buffer to help preserve chaperone-client interactions. Samples were analyzed on an AB SCIEX 5600 TripleTOF system by data-dependent acquisition (DDA). See Extended Experimental Procedures for details and for AP-MS data analysis.

Hierarchical Clustering

Cochaperones and client proteins were organized by hierarchical clustering with average linkage and centered Pearson correlation. Only bait proteins that were detectably expressed (as measured by ELISA) in at least 50 of the 60 experiments were included in the analysis.

Data Sets

All data sets can be accessed online at http://prohits-web.lunenfeld.ca. All interactions have also been submitted to BioGRID and the IMEx consortium (www.imexconsortium.org) through IntAct (Orchard et al., 2014) and assigned the identifier IM-22301.

SUPPLEMENTAL INFORMATION

Supplemental Information includes Extended Experimental Procedures, six figures, and one table and can be found with this article online at http://dx.doi.org/10.1016/j.cell.2014.05.039.

AUTHOR CONTRIBUTIONS

M.T., S.L., and A.-C.G. conceived the project and designed experiments. M.T. and I.K. established stable cell lines and performed all LUMIER assays. Z.-Y.L. performed AP-MS experiments. B.L. provided mass spectrometry guidance to Z.Y.L. and helped develop the AP-MS method. G.T. and J.P., supervised by B.B., developed the LUMIER scoring algorithm and J.P. performed coevolutionary analyses. H.C. performed statistical analyses of AP-MS data. M.T. and S.L. wrote the paper with significant contributions from A.-C.G., G.T., and J.P.

ACKNOWLEDGMENTS

We thank Y. Freyzon and M. Fischer for technical help, M. Shair for OSW-1, and A. Nesvizhskii and members of S.L. and A.-C.G.'s labs for comments and suggestions. We are grateful to M. Vidal and D. Hill for providing the human ORFeome. The website http://prohits-web.lunenfeld.ca is designed and maintained by J. Zhang and G. Liu. This work was supported by the Canadian Institutes of Health Research (MOP-84314 to A.-C.G.) and the NIH (5R01GM94231 to A.-C.G. and GM081871 to B.B.). M.T. was supported by the HFSP and a Margaret and Herman Sokol Postdoctoral Award. A.-C.G. holds the Canada Chair in Functional Proteomics and the Lea Reichmann Chair in Cancer Proteomics. S.L. is an investigator of the Howard Hughes Medical Institute.

Received: October 21, 2013
Revised: March 8, 2014
Accepted: May 16, 2014
Published: July 17, 2014

REFERENCES

Barrios-Rodiles, M., Brown, K.R., Ozdamar, B., Bose, R., Liu, Z., Donovan, R.S., Shinjo, F., Liu, Y., Dembowy, J., Taylor, I.W., et al. (2005). High-throughput mapping of a dynamic signaling network in mammalian cells. Science *307*, 1621–1625.

Bengtson, M.H., and Joazeiro, C.A.P. (2010). Role of a ribosome-associated E3 ubiquitin ligase in protein quality control. Nature *467*, 470–473.

Braun, P., Tasan, M., Dreze, M., Barrios-Rodiles, M., Lemmens, I., Yu, H., Sahalie, J.M., Murray, R.R., Roncari, L., de Smet, A.-S., et al. (2009). An experimentally derived confidence score for binary protein-protein interactions. Nat. Methods *6*, 91–97.

Briknarová, K., Takayama, S., Homma, S., Baker, K., Cabezas, E., Hoyt, D.W., Li, Z., Satterthwait, A.C., and Ely, K.R. (2002). BAG4/SODD protein contains a short BAG domain. J. Biol. Chem. *277*, 31172–31178.

Brychzy, A., Rein, T., Winklhofer, K.F., Hartl, F.U., Young, J.C., and Obermann, W.M.J. (2003). Cofactor Tpr2 combines two TPR domains and a J domain to regulate the Hsp70/Hsp90 chaperone system. EMBO J. *22*, 3613–3623.

Burgett, A.W.G., Poulsen, T.B., Wangkanont, K., Anderson, D.R., Kikuchi, C., Shimada, K., Okubo, S., Fortner, K.C., Mimaki, Y., Kuroda, M., et al. (2011). Natural products reveal cancer cell dependence on oxysterol-binding proteins. Nat. Chem. Biol. *7*, 639–647.

Calloni, G., Chen, T., Schermann, S.M., Chang, H.-C., Genevaux, P., Agostini, F., Tartaglia, G.G., Hayer-Hartl, M., and Hartl, F.U. (2012). DnaK functions as a central hub in the E. coli chaperone network. Cell Rep. *1*, 251–264.

Chadli, A., Felts, S.J., and Toft, D.O. (2008). GCUNC45 is the first Hsp90 co-chaperone to show alpha/beta isoform specificity. J. Biol. Chem. *283*, 9509–9512.

Chaudhuri, I., Söding, J., and Lupas, A.N. (2008). Evolution of the beta-propeller fold. Proteins *71*, 795–803.

Cotta-Ramusino, C., McDonald, E.R., 3rd, Hurov, K., Sowa, M.E., Harper, J.W., and Elledge, S.J. (2011). A DNA damage response screen identifies RHINO, a 9-1-1 and TopBP1 interacting protein required for ATR signaling. Science *332*, 1313–1317.

Echtenkamp, F.J., and Freeman, B.C. (2012). Expanding the cellular molecular chaperone network through the ubiquitous cochaperones. Biochim. Biophys. Acta *1823*, 668–673.

Echtenkamp, F.J., Zelin, E., Oxelmark, E., Woo, J.I., Andrews, B.J., Garabedian, M., and Freeman, B.C. (2011). Global functional map of the p23 molecular chaperone reveals an extensive cellular network. Mol. Cell *43*, 229–241.

Eisen, M.B., Spellman, P.T., Brown, P.O., and Botstein, D. (1998). Cluster analysis and display of genome-wide expression patterns. Proc. Natl. Acad. Sci. USA *95*, 14863–14868.

Eulalio, A., Behm-Ansmant, I., and Izaurralde, E. (2007). P bodies: at the crossroads of post-transcriptional pathways. Nat. Rev. Mol. Cell Biol. *8*, 9–22.

Finley, D. (2009). Recognition and processing of ubiquitin-protein conjugates by the proteasome. Annu. Rev. Biochem. *78*, 477–513.

Freeman, B.C., Toft, D.O., and Morimoto, R.I. (1996). Molecular chaperone machines: chaperone activities of the cyclophilin Cyp-40 and the steroid aporeceptor-associated protein p23. Science *274*, 1718–1720.

Fuchs, M., Poirier, D.J., Seguin, S.J., Lambert, H., Carra, S., Charette, S.J., and Landry, J. (2010). Identification of the key structural motifs involved in HspB8/HspB6-Bag3 interaction. Biochem. J. *425*, 245–255.

Gano, J.J., and Simon, J.A. (2010). A proteomic investigation of ligand-dependent HSP90 complexes reveals CHORDC1 as a novel ADP-dependent HSP90-interacting protein. Mol. Cell. Proteomics *9*, 255–270.

Hudson, A.M., and Cooley, L. (2008). Phylogenetic, structural and functional relationships between WD- and Kelch-repeat proteins. Subcell. Biochem. *48*, 6–19.

Iwasaki, S., Kobayashi, M., Yoda, M., Sakaguchi, Y., Katsuma, S., Suzuki, T., and Tomari, Y. (2010). Hsc70/Hsp90 chaperone machinery mediates ATP-dependent RISC loading of small RNA duplexes. Mol. Cell *39*, 292–299.

Jagannathan, M., Sakwe, A.M., Nguyen, T., and Frappier, L. (2012). The MCM-associated protein MCM-BP is important for human nuclear morphology. J. Cell Sci. *125*, 133–143.

Jarosz, D.F., Taipale, M., and Lindquist, S. (2010). Protein homeostasis and the phenotypic manifestation of genetic diversity: principles and mechanisms. Annu. Rev. Genet. *44*, 189–216.

Kadota, Y., Shirasu, K., and Guerois, R. (2010). NLR sensors meet at the SGT1-HSP90 crossroad. Trends Biochem. Sci. *35*, 199–207.

Kampinga, H.H., and Craig, E.A. (2010). The HSP70 chaperone machinery: J proteins as drivers of functional specificity. Nat. Rev. Mol. Cell Biol. *11*, 579–592.

Kean, M.J., Couzens, A.L., and Gingras, A.-C. (2012). Mass spectrometry approaches to study mammalian kinase and phosphatase associated proteins. Methods *57*, 400–408.

Kundrat, L., and Regan, L. (2010). Balance between folding and degradation for Hsp90-dependent client proteins: a key role for CHIP. Biochemistry *49*, 7428–7438.

Lander, G.C., Estrin, E., Matyskiela, M.E., Bashore, C., Nogales, E., and Martin, A. (2012). Complete subunit architecture of the proteasome regulatory particle. Nature *482*, 186–191.

Lukov, G.L., Baker, C.M., Ludtke, P.J., Hu, T., Carter, M.D., Hackett, R.A., Thulin, C.D., and Willardson, B.M. (2006). Mechanism of assembly of G protein betagamma subunits by protein kinase CK2-phosphorylated phosducin-like protein and the cytosolic chaperonin complex. J. Biol. Chem. *281*, 22261–22274.

Lundin, V.F., Leroux, M.R., and Stirling, P.C. (2010). Quality control of cytoskeletal proteins and human disease. Trends Biochem. Sci. *35*, 288–297.

Orchard, S., Ammari, M., Aranda, B., Breuza, L., Briganti, L., Broackes-Carter, F., Campbell, N.H., Chavali, G., Chen, C., del-Toro, N., et al. (2014). The MIntAct project—IntAct as a common curation platform for 11 molecular interaction databases. Nucleic Acids Res. *42*, D358–D363.

Powers, E.T., and Balch, W.E. (2013). Diversity in the origins of proteostasis networks—a driver for protein function in evolution. Nat. Rev. Mol. Cell Biol. *14*, 237–248.

Powers, E.T., Morimoto, R.I., Dillin, A., Kelly, J.W., and Balch, W.E. (2009). Biological and chemical approaches to diseases of proteostasis deficiency. Annu. Rev. Biochem. *78*, 959–991.

Saibil, H. (2013). Chaperone machines for protein folding, unfolding and disaggregation. Nat. Rev. Mol. Cell Biol. *14*, 630–642.

Schmid, A.B., Lagleder, S., Gräwert, M.A., Röhl, A., Hagn, F., Wandinger, S.K., Cox, M.B., Demmer, O., Richter, K., Groll, M., et al. (2012). The architecture of functional modules in the Hsp90 co-chaperone Sti1/Hop. EMBO J. *31*, 1506–1517.

Scholz, G.M., Cartledge, K., and Hall, N.E. (2001). Identification and characterization of Harc, a novel Hsp90-associating relative of Cdc37. J. Biol. Chem. *276*, 30971–30979.

Schuyler, S.C., Wu, Y.-F., and Kuan, V.J.-W. (2012). The Mad1-Mad2 balancing act—a damaged spindle checkpoint in chromosome instability and cancer. J. Cell Sci. *125*, 4197–4206.

Shao, J., Irwin, A., Hartson, S.D., and Matts, R.L. (2003). Functional dissection of cdc37: characterization of domain structure and amino acid residues critical for protein kinase binding. Biochemistry *42*, 12577–12588.

Taipale, M., Jarosz, D.F., and Lindquist, S. (2010). HSP90 at the hub of protein homeostasis: emerging mechanistic insights. Nat. Rev. Mol. Cell Biol. *11*, 515–528.

Taipale, M., Krykbaeva, I., Koeva, M., Kayatekin, C., Westover, K.D., Karras, G.I., and Lindquist, S. (2012). Quantitative analysis of HSP90-client interactions reveals principles of substrate recognition. Cell *150*, 987–1001.

Taipale, M., Krykbaeva, I., Whitesell, L., Santagata, S., Zhang, J., Liu, Q., Gray, N.S., and Lindquist, S. (2013). Chaperones as thermodynamic sensors of drug-target interactions reveal kinase inhibitor specificities in living cells. Nat. Biotechnol. *31*, 630–637.

Teo, G., Liu, G., Zhang, J., Nesvizhskii, A.I., Gingras, A.-C., and Choi, H. (2014). SAINTexpress: improvements and additional features in Significance Analysis of INTeractome software. J. Proteomics *100*, 37–43.

Tokuriki, N., and Tawfik, D.S. (2009). Chaperonin overexpression promotes genetic variation and enzyme evolution. Nature *459*, 668–673.

Tong, A.H.Y., Lesage, G., Bader, G.D., Ding, H., Xu, H., Xin, X., Young, J., Berriz, G.F., Brost, R.L., Chang, M., et al. (2004). Global mapping of the yeast genetic interaction network. Science *303*, 808–813.

Trepel, J., Mollapour, M., Giaccone, G., and Neckers, L. (2010). Targeting the dynamic HSP90 complex in cancer. Nat. Rev. Cancer *10*, 537–549.

Tsukahara, F., and Maru, Y. (2010). Bag1 directly routes immature BCR-ABL for proteasomal degradation. Blood *116*, 3582–3592.

Xu, W., Marcu, M., Yuan, X., Mimnaugh, E., Patterson, C., and Neckers, L. (2002). Chaperone-dependent E3 ubiquitin ligase CHIP mediates a degradative pathway for c-ErbB2/Neu. Proc. Natl. Acad. Sci. USA *99*, 12847–12852.

Yam, A.Y., Xia, Y., Lin, H.-T.J., Burlingame, A., Gerstein, M., and Frydman, J. (2008). Defining the TRiC/CCT interactome links chaperonin function to stabilization of newly made proteins with complex topologies. Nat. Struct. Mol. Biol. *15*, 1255–1262.

Ying, W., Du, Z., Sun, L., Foley, K.P., Proia, D.A., Blackman, R.K., Zhou, D., Inoue, T., Tatsuta, N., Sang, J., et al. (2012). Ganetespib, a unique triazolone-containing Hsp90 inhibitor, exhibits potent antitumor activity and a superior safety profile for cancer therapy. Mol. Cancer Ther. *11*, 475–484.

Zhao, R., Davey, M., Hsu, Y.-C., Kaplanek, P., Tong, A., Parsons, A.B., Krogan, N., Cagney, G., Mai, D., Greenblatt, J., et al. (2005). Navigating the chaperone network: an integrative map of physical and genetic interactions mediated by the hsp90 chaperone. Cell *120*, 715–727.

Zheng, M., Cierpicki, T., Burdette, A.J., Utepbergenov, D., Janczyk, P.Ł., Derewenda, U., Stukenberg, P.T., Caldwell, K.A., and Derewenda, Z.S. (2011). Structural features and chaperone activity of the NudC protein family. J. Mol. Biol. *409*, 722–741.